JACS
JOURNAL OF THE AMERICAN CHEMICAL SOCIETY

Communication

pubs.acs.org/JACS

Reversible Assembly of Stacked Membrane Nanodiscs with Reduced Dimensionality and Variable Periodicity

Paul A. Beales,*[,†] Nienke Geerts,[‡] Krishna K. Inampudi,[‡] Hideki Shigematsu,[∥] Corey J. Wilson,[‡] and T. Kyle Vanderlick*[,‡]

[†]Centre for Molecular Nanoscience, School of Chemistry, University of Leeds, Leeds LS2 9JT, U.K.

[‡]Department of Chemical and Environmental Engineering and [∥]Department of Cellular and Molecular Physiology, Yale University, New Haven, Connecticut 06510, United States

Supporting Information

ABSTRACT: We demonstrate the self-organization of quasi-one-dimensional nanostructures with periodic features using nature's primary three building blocks: lipids, DNA, and proteins. The periodicity of these "BioNanoStacks" is controllable through selection of the length of the DNA spacers. We show that BioNanoStacks can be reversibly assembled and disassembled through thermal melting of the DNA duplex, where the melting transition temperature is controllable not just by the DNA sequence and salt concentration, but also by the lipid composition within these superstructures. These novel materials may find applications in fields such as templated nanomaterial assembly, tissue-engineering scaffolds, or therapeutic delivery systems. Well-established techniques for chemical modification of biomolecules will also provide a broad platform for adaption and remodeling of these structures to provide optimal features for the required application.

From skyscrapers to nacre,[1] trains to optical gratings, and ladders to quantum cascade lasers,[2] stacked structures are commonplace in materials and devices across all length scales. The stacking arrangements can yield advantageous properties such as directional transport, signal amplification and enhanced mechanical strength. In this paper, we demonstrate the assembly of regular stacks of planar biomembrane discs on nanometer length scales. These novel architectures have controllable structural features on length scales below 10 nm, which is, at present, the lower limit of the most advanced lithographic fabrication techniques.[3]

The "BioNanoStacks" we introduce here take advantage of nature's three main structural components: lipids, proteins, and nucleic acids (Figure 1). Lipids assemble into bilayer discs, stabilized by scaffold proteins.[4] Lipid−DNA conjugates inserted into the bilayer nanodiscs act as molecular glue: the nucleic acid sequences extend from the membrane surface and are free to bind their complement. Mixtures of nanodiscs functionalized with complementary DNA assemble into columnar membrane stacks with a periodic structure. This architecture is favored due to the shape anisotropy of bilayer discs and the relative orientations of the DNA. The BioNanoStacks that form are materials of reduced dimensionality, consisting of nanoscale two-dimensional membrane discs, whose diameters are regulated by the scaffold protein, assembled into a quasi-one-dimensional strings by the DNA.

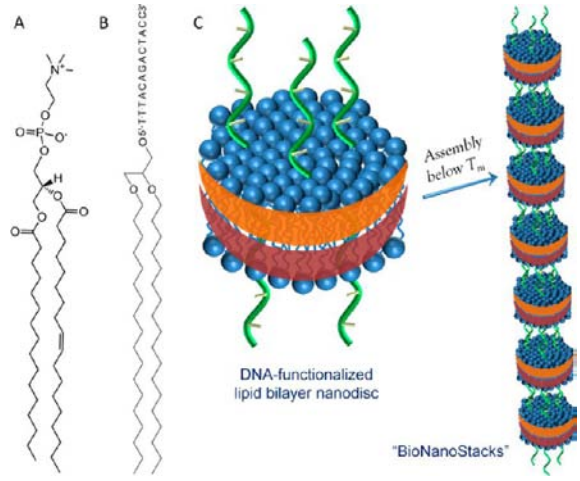

Figure 1. Structures of (A) POPC and (B) the dialkyl lipid anchor for the DNA sequences with the sequence of LDNA1 shown, where the anchor links to the 5′ end of the sequence. (C) Cartoon depiction of a lipid bilayer (blue) nanodisc stabilized by two MSP1D1 α-helical scaffold proteins (red, orange) and functionalized with lipid−DNA (green). Below the T_m of the DNA duplex, these nanodiscs self-assemble with nanodiscs functionalized with complementary DNA strands to form BioNanoStacks.

Lipid nanodiscs are constructed from the self-assembly of lipids with membrane scaffold proteins that form amphiphatic α-helical ribbons that stabilize the line tension at the lipid bilayer edge, thus forming stable disc-shaped micelles with low size dispersity.[5] The scaffold protein we use was developed by Sligar's group and is a derivative of apolipoprotein A-1.[5] The membrane scaffold protein (MSP1D1) was expressed in the BL21 (DE3) *E. coli* strain and purified by affinity chromatography on a Ni-column by virtue of the protein's 7 histidine tag.[6] Protein purity was checked by SDS-PAGE (e.g., Figure S1). Lipids (POPC) are dispersed in sample buffer (20 mM Tris, 100 mM NaCl; pH 7.4) containing 40 mM sodium cholate to form a clear sample of mixed POPC/cholate micelles. MSP1D1 in sample buffer is added to a final protein:lipid:cholate ratio of

Received: November 26, 2012
Published: February 13, 2013

   dx.doi.org/10.1021/ja311561d | *J. Am. Chem. Soc.* 2013, 135, 3335−3338

1:65:100 and mixed at 4 °C for 1 h. Cholate surfactant is then removed by incubating the sample on Bio-beads SM2 for 4−6 h at 4 °C, before careful removal of the nanodisc sample from these absorbant beads.

Nanodisc formation is analyzed by size exclusion chromatography on a Superdex 200 GL 10/300 column: nanodisc samples elute at an apparent M_w of 142 ± 19 kDa (with a similar peak width to 150 kDa alcohol dehydrogenase, used as a M_w standard for column calibration, also suggesting a narrow size distribution) (see Figure S2). This apparent size is consistent with two proteins and ∼130 lipids per nanodisc (∼148 kDa). Lipid concentration in these samples was measured using a total phosphorus assay.

Two populations of lipid nanodiscs are then functionalized by complementary DNA−lipid conjugates. Dialkyl lipid phosphoramidite precursors are synthesized as previously described.[7,8] These are added as the final base on a conventional DNA synthesizer to create the two 13mer lipid-DNA hybrid molecules: LDNA1 (lipid-5′-TTT ACA GAC TAC C-3′) and LDNA2 (lipid-5′-TTT GGT AGT CTG T-3′); successful conjugation was checked by mass spectroscopy (Figure S3). Each lipid−DNA was mixed with an aliquot of the nanodisc sample at mean functionalization ratios of ⟨4⟩ or ⟨6⟩ DNA per nanodisc for a minimum of 45 min to allow bilayer functionalization to occur.

BioNanoStacks are formed by slow cooling of a binary (complementary) population of functionalized nanodiscs. Equivalent proportions of LDNA1- and LDNA2-functionalized nanodiscs are mixed at a final nanodisc concentration of between 2 and 4 μM. The samples are then rapidly heated to 60 °C (a temperature at which the DNA strands do not hybridize[9] and the nanodiscs are known to still be stable[10]) in a Cary 100 Biomelt UV−vis spectrophotometer and then slowly cooled at −0.1 °C/min back to room temperature so as to allow the DNA-functionalized nanodiscs to self-organize into near-equilibrium superstructures.

The resultant superstructures can reach sizes resolvable under an optical microscope and a string-like morphology from the nanodisc stacking is apparent on this length scale. First, 100 μL of the BioNanoStack sample is mixed on a BSA-treated glass-bottomed culture dish with 1.0 μL of 0.1 mg mL^{-1} Rh-DOPE in DMSO, prior to observation. The Rh-DOPE probe rapidly diffused into the lipid structures allowing direct observation of their microscale morphology (Figure 2a−d). Multi-micrometer-sized structures with a string-like texture are clearly visible. In comparison, the DNA-mediated adhesion between spherically symmetric, 100 nm liposomes yields 3D, "cloud-like" assemblies (Figure 2e). However, higher resolution imaging is required to confirm the nanoscale structure of the assembled nanodisc architectures.

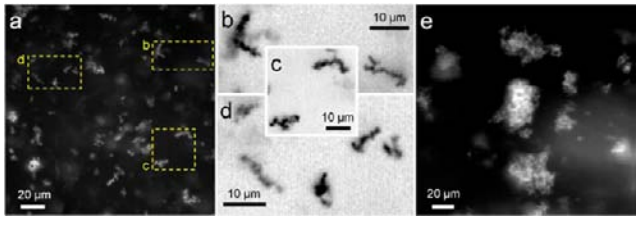

Figure 2. (a) Epifluorescence microscopy image of BioNanoStacks labeled with Rh-DOPE; 2 μM mixed population of POPC nanodiscs functionalized with LDNA1 and LDNA2 at a mean loading of ⟨4⟩ DNA per nanodisc in 50 mM NaCl buffer (room temperature). (b−d) Magnified, negative contrast regions, highlighted by yellow dashed boxes in part a. (e) Microscale morphology of POPC liposomes assembled via DNA linkers.

Negative-staining transmission electron microscopy (TEM) confirms the nanodisc stacking structure through hybridization of complementary DNA functionalities. TEM grids are prepared and stained using Nano-W (Nanoprobes, Inc.). Quasi-1D self-assembly of DNA-functionalized nanodiscs is conclusively observed in these TEM micrographs (Figure 3a−d). BioNanoStack morphologies are reminiscent of those previously reported for self-organized prismatic inorganic nanoparticles.[11] No stacked nanostructures were evident in control samples of unfunctionalized nanodiscs at the TEM grid preparation concentration (0.4−0.8 μM nanodiscs). High aspect ratio linear stacks with large apparent persistence lengths are seen in the ionic strength range 50−100 mM NaCl. The BioNanoStacks observed by TEM grow up to many tens of nanodiscs in lengths, with branching events during growth appearing to be rare. As these samples for TEM were created by adsorption of BioNanoStacks onto a TEM grid, overlapping of adsorbed structures could occur, giving the appearance of branching or higher order assemblies (e.g., Figure 3c,d). (We estimate BioNanoStack yield to be >95% across all samples.) The largest multi-micrometer structures observable by optical microscopy (Figure 2) are likely not seen by TEM due to the nature of the sample preparation: TEM grids are placed on top of the sample droplet to allow BioNanoStacks to absorb; the largest superstructures will sediment toward the bottom of the droplet, significantly reducing the probability of them adsorbing onto the TEM sample grids. Analysis of our TEM micrographs reveals a mean apparent nanodisc repeat unit of 5.6 ± 0.3 nm. This is less than the expected spacing of ∼9−10 nm (based upon a ∼5 nm bilayer and 13-base DNA linkers), likely due to dehydration of the sample during TEM grid preparation, reducing the apparent inter-nanodisc spacing.

To remove the possibility of drying artifacts in the observed periodicity of BioNanoStacks using negative-staining TEM, cryo-TEM was used to analyze samples (Figure 3e,f). Cryo-TEM images were also used to measure the apparent nanodisc dimensions: 11.9 ± 1.8 nm diameter and 5.7 ± 0.4 nm thickness (101 nanodiscs analyzed); these results are slightly larger than reported values for DPPC-MSP1D1 nanodiscs (9.7 and 5.7 nm, respectively) measured by SAXS.[5] BioNanoStacks assembled using the 13mer LDNA1 and LDNA2 pair (Figure 3e) were found to be separated by 4.7 ± 0.6 nm (excluding nanodisc thickness). Based upon an estimated contour length of 0.34 nm per base,[12] this is consistent with a separation distance of 14 DNA bases. Note that only 10 bases are hybridized and 3 overlapping bases are at each end, i.e., 16 bases in length; therefore, this suggests that the interconnecting DNA linkers tilt at only a slight angle to the bilayer normal.

To demonstrate that inter-nanodisc spacing is controllable through the length of the DNA spacer, we formed BioNanoStacks using the complementary 23mer DNA pair LDNA3 and LDNA4 (Figure 3f). Here we measure an inter-nanodisc spacing of 7.8 ± 1.1 nm (comparable to the length of 23 DNA bases). The difference in spacing between the 13mer and 23mer DNA spacers is consistent with a length difference of 9 DNA bases (almost the maximum physical difference in nanodisc separation, equivalent to 10 base pairs in length). This supports our earlier conclusion that DNA linkers between

dx.doi.org/10.1021/ja311561d | J. Am. Chem. Soc. 2013, 135, 3335−3338

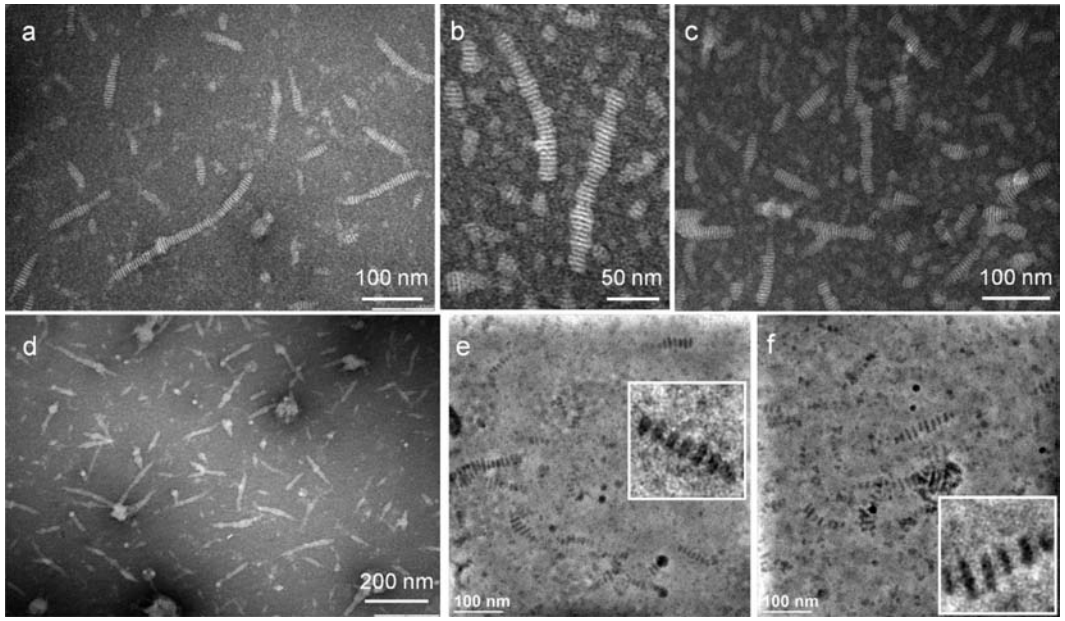

Figure 3. TEM images of BioNanoStacks. (a–d) TEM micrographs of BioNanoStacks after negative staining with Nano-W: (a,d) 400 nM mixed population of POPC nanodiscs with a mean DNA loading of 4 per nanodisc (LDNA1 or LDNA2) assembled in a 100 mM NaCl buffer; (b,c) 800 nM mixed population of POPC nanodiscs with a mean DNA loading of 4 per nanodisc (LDNA1 or LDNA2) assembled in a 75 mM NaCl buffer. (e,f) Cryo-TEM of 4 μM BioNanoStacks assembled in a 50 mM NaCl buffer (insets show magnified BioNanoStack structures): (e) nanodiscs functionalized with a mean DNA loading of 4 per nanodisc (13mers LDNA1 and LDNA2); (f) nanodiscs functionalized with a mean DNA loading of 4 per nanodisc (23mers LDNA3 and LDNA4).

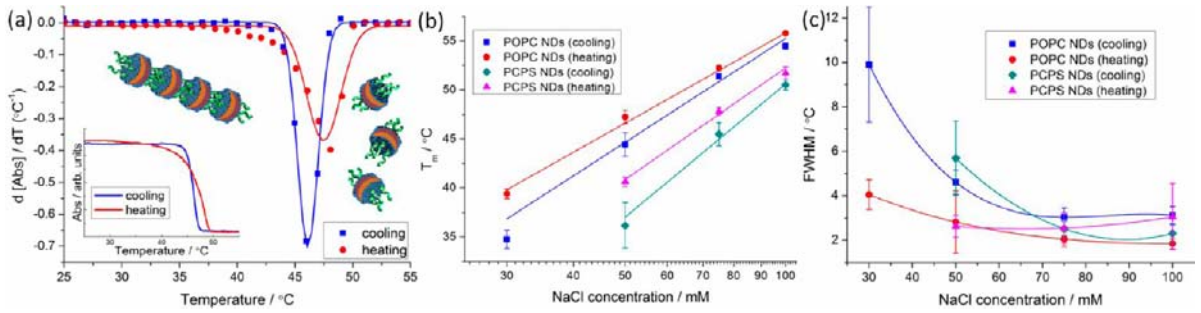

Figure 4. Thermal melting studies of BioNanoStacks. (a) Examples of melting analysis for cooling and heating temperature cycles for 4 μM PCPS nanodiscs functionalized with <6> 13mer DNA/nanodisc in 75 mM NaCl. The inset shows the UV melting curves. The first derivative is then taken and fit to a Gaussian function. The peak position of this fit is taken to be the T_m and the fwhm is taken to be a measure of the width (i.e., cooperativity) of the melting transition. (b) Graph of T_m against salt concentration (c_s) for POPC and PCPS nanodiscs; fitting trends assume $T_m \propto \ln c_s$. (c) Graph of fwhm against salt concentration for POPC and PCPS nanodiscs; fitting curves are intended to guide the eyes to the trends. Heating and cooling cycles are analyzed independently. Error bars are calculated as $\pm 1\sigma$ from the mean.

nanodiscs sit almost perpendicular to the membrane, with only a small tilt angle to the bilayer normal.

Melting temperatures (T_m) of the BioNanoStacks due to reversible DNA hybridization were measured for a range of ionic strengths and lipid compositions. UV spectroscopy at 320 nm (a wavelength at which DNA does not absorb) was used to monitor the change in sample turbidity due to nanodisc assembly during heating and cooling cycles (0.1 °C min^{-1}). We have previously compared the T_m of unmodified DNAs with those functionalized on liposomes;[9] DNA-functionalized nanoparticles melt at higher T_m than the pristine DNA due to the requirement of cooperative melting of multiple strands and multivalent interactions between surfaces. The first derivatives of these melting curves were calculated to obtain the T_m and width (or cooperativity) of the transition (full width at half-maximum; fwhm) (Figure 4a). Four heating and cooling cycles were performed on each sample over a period of ~3 days; no loss in reversibility of the assembly process was observed during these scans, demonstrating the stability of these soft nanostructures to multiple annealing cycles. Some hysteresis is observed between heating and cooling cycles with T_m consistently higher for heating cycles than cooling cycles. Heating cycles usually also exhibit sharper melting transitions (lower fwhm, or greater cooperativity) than cooling cycles; this is likely due to the requirement of the cooperative dissociation of multiple DNA bonds for the nanodiscs to become detached from one another, whereas only a single DNA bond needs to form for two nanodiscs to assemble during the cooling cycle.

As expected, DNA T_m decreased with decreasing NaCl concentration due to the requirement of counterions to screen electrostatic repulsion between the sugar–phosphate backbones (Figure 4b). We find that over the range of salt concentrations (c_s) we study, a model of $T_m \propto \ln c_s$ is sufficient to describe the trends in our data. However this should be

dx.doi.org/10.1021/ja311561d | J. Am. Chem. Soc. 2013, 135, 3335–3338

treated as a phenomenological fit: even for simple DNA duplexes alone, determining the precise functional form of the $[Na^+]$ dependence of T_m is a challenging problem.[13]

We find that nanodiscs containing anionic lipids (1:1 POPC:POPS; denoted PCPS) melt at lower temperatures than those composed purely of zwitterionic POPC, neutral under our experimental conditions (Figure 4b). This is consistent with our previous report that the T_m for DNA-linked liposomes can be dependent on the lipid composition.[9] We rationalize this as being due to inter-membrane repulsion between anionic membranes reducing the hybridization free energy of the DNA duplexes that act as "adhesion receptors" binding them together. Finally, we note that the melting transitions are relatively sharp (2−3 °C) at higher c_s (Figure 4c), as has been demonstrated for the DNA-mediated assembly of other nanomaterials.[14] However, the cooperativity of the transition decreases (an increase in fwhm) with decreasing c_s; this trend is particularly significant during sample cooling (nanodisc assembly).

Living organisms harness biomolecular self-organization to construct and manipulate intricate superstructures and machinery at the nanoscale. Here we demonstrate assembly of quasi-1D biomembrane stacks of fixed diameter and controlled chemical periodicity on sub-10 nm length scales. Inspiration has been taken from nature to create novel materials derived from its fundamental building blocks (lipids, proteins, DNA). This builds on recent work that has used the successful marriage of lipids and DNA into functional conjugates for assembly of new soft materials.[8,15−20] The reduced dimensionality of these nanostructures is derived from the nonspherical symmetry of the structural building block, namely the nanodisc. Breaking the spherical symmetry of building blocks[21,22] to be assembled by DNA−lipids has previously been demonstrated to increase control over the resultant superstructures that can be assembled using Janus-textured vesicles.[7] Controlled manipulation of the size, shape and interactions of supramolecular building blocks opens up broad possibilities for material self-assembly at the nanoscale.

These novel nanoarchitectures could find many applications in materials and device design. The array of chemical modifications and material assembly protocols that can now be applied to lipids,[23] proteins,[24] and DNA[25,26] provides a variety of available strategies for incorporation of additional functionalities into BioNanoStack architectures. Inclusion of integral membrane proteins into nanodiscs[27] could be a strategy for assembly of linear arrays of proteins for serial signal transduction in biosynthetic devices (e.g., long-range ion/charge transport). The periodic nature of BioNanoStacks could also be used as templates for the fabrication of inorganic materials, e.g., assembling regular 1D arrays of nanoparticles or templating biomimetic mineral growth. Furthermore incorporation of therapeutic compounds or growth factors into these materials may also offer exciting new opportunities in drug delivery or tissue engineering. Therefore, directing assembly of such nature-inspired materials with controlled shape, composition, and dimensions is desirable for realization of a range of technologies on nanometer length scales.

■ ASSOCIATED CONTENT

Supporting Information

Materials and methods, SDS-PAGE of MSP1D1 protein, size exclusion chromatography data of nanodiscs, and mass spectra of DNA−lipids. This material is available free of charge via the Internet at http://pubs.acs.org.

■ AUTHOR INFORMATION

Corresponding Author

p.a.beales@leeds.ac.uk; kyle.vanderlick@yale.edu

Notes

The authors declare no competing financial interest.

■ ACKNOWLEDGMENTS

We thank Dr. Abhinav Nath and Joanna Dunn for helpful discussions on nanodisc assembly and characterization. We thank Dr. Jin Nam for assistance with the lipid phosphoramidite synthesis. We also acknowledge Prof. Fred Sigworth, Dr. Christoph Rahner, and Morven Graham at the electron microscopy facility in Yale School of Medicine as well as the Keck Facility at Yale for support and assistance.

■ REFERENCES

(1) Tang, Z. Y.; Kotov, N. A.; Magonov, S.; Ozturk, B. *Nat. Mater.* **2003**, *2*, 413.
(2) Faist, J.; Capasso, F.; Sivco, D. L.; Sirtori, C.; Hutchinson, A. L.; Cho, A. Y. *Science* **1994**, *264*, 553.
(3) Vieu, C.; Carcenac, F.; Pepin, A.; Chen, Y.; Mejias, M.; Lebib, A.; Manin-Ferlazzo, L.; Couraud, L.; Launois, H. *Appl. Surf. Sci.* **2000**, *164*, 111.
(4) Nath, A.; Atkins, W. M.; Sligar, S. G. *Biochemistry* **2007**, *46*, 2059.
(5) Denisov, I. G.; Grinkova, Y. V.; Lazarides, A. A.; Sligar, S. G. *J. Am. Chem. Soc.* **2004**, *126*, 3477.
(6) Ritchie, T. K.; Grinkova, Y. V.; Bayburt, T. H.; Denisov, I. G.; Zolnerciks, J. K.; Atkins, W. M.; Sligar, S. G. *Methods Enzymol.* **2009**, *464*, 211.
(7) Beales, P. A.; Nam, J.; Vanderlick, T. K. *Soft Matter* **2011**, *7*, 1747.
(8) Chan, Y.-H. M.; van Lengerich, B.; Boxer, S. G. *Biointerphases* **2008**, *3*, FA17.
(9) Beales, P. A.; Vanderlick, T. K. *Biophys. J.* **2009**, *96*, 1554.
(10) Shaw, A. W.; McLean, M. A.; Sligar, S. G. *FEBS Lett.* **2004**, *556*, 260.
(11) Li, M.; Schnablegger, H.; Mann, S. *Nature* **1999**, *402*, 393.
(12) Smith, S. B.; Cui, Y. J.; Bustamante, C. *Science* **1996**, *271*, 795.
(13) Owczarzy, R.; You, Y.; Moreira, B. G.; Manthey, J. A.; Huang, L. Y.; Behlke, M. A.; Walder, J. A. *Biochemistry* **2004**, *43*, 3537.
(14) Jin, R. C.; Wu, G. S.; Li, Z.; Mirkin, C. A.; Schatz, G. C. *J. Am. Chem. Soc.* **2003**, *125*, 1643.
(15) Beales, P. A.; Vanderlick, T. K. *J. Phys. Chem. A* **2007**, *111*, 12372.
(16) Berti, D.; Montis, C.; Baglioni, P. *Soft Matter* **2011**, *7*, 7150.
(17) Bunge, A.; Loew, M.; Pescador, P.; Arbuzova, A.; Brodersen, N.; Kang, J.; Daehne, L.; Liebscher, J.; Herrmann, A.; Stengel, G.; Huster, D. *J. Phys. Chem. B* **2009**, *113*, 16425.
(18) Dave, N.; Liu, J. *Chem. Commun.* **2012**, *48*, 3718.
(19) Kwak, M.; Herrmann, A. *Chem. Soc. Rev.* **2011**, *40*, 5745.
(20) Patwa, A.; Gissot, A.; Bestel, I.; Barthelemy, P. *Chem. Soc. Rev.* **2011**, *40*, 5844.
(21) Beales, P. A.; Vanderlick, T. K. *J. Phys. Chem. B* **2009**, *113*, 13678.
(22) Loew, M.; Springer, R.; Scolari, S.; Altenbrunn, F.; Seitz, O.; Liebscher, J.; Huster, D.; Herrmann, A.; Arbuzova, A. *J. Am. Chem. Soc.* **2010**, *132*, 16066.
(23) Zhang, X.-X.; McIntosh, T. J.; Grinstaff, M. W. *Biochimie* **2012**, *94*, 42.
(24) Basle, E.; Joubert, N.; Pucheault, M. *Chem. Biol.* **2010**, *17*, 213.
(25) Jager, S.; Rasched, G.; Kornreich-Leshem, H.; Engeser, M.; Thum, O.; Famulok, M. *J. Am. Chem. Soc.* **2005**, *127*, 15071.
(26) Pinheiro, A. V.; Han, D.; Shih, W. M.; Yan, H. *Nature Nanotechnol.* **2011**, *6*, 763.
(27) Bayburt, T. H.; Sligar, S. G. *FEBS Lett.* **2010**, *584*, 1721.